Zero temperature phase diagram of the square-shoulder system

Gernot J. Pauschenwein[a] and Gerhard Kahl
Institut für Theoretische Physik and Center for Computational Materials Science (CMS), Technische Universität Wien, Wiedner Hauptstraße 8-10, A-1040 Wien, Austria

(Received 30 July 2008; accepted 1 October 2008; published online 6 November 2008)

Particles that interact via a square-shoulder potential, consisting of an impenetrable hard core with an adjacent, repulsive, steplike corona, are able to self-organize in a surprisingly rich variety of rather unconventional ordered, three-dimensional structures. Using optimization strategies that are based on ideas of genetic algorithms, we encounter, as we systematically increase the pressure, the following archetypes of aggregates: low-symmetry cluster and columnar phases, followed by lamellar particle arrangements, until at high pressure values compact, high-symmetry lattices emerge. These structures are characterized in the isobaric-isothermal ensemble as configurations of minimum Gibbs free energy. Based on simple considerations, i.e., basically minimizing the number of overlapping coronas while maximizing at the same time the density, the sequence of emerging structures can easily be understood. In contrast to a previous contribution [G. J. Pauschenwein and G. Kahl, Soft Matter **4**, 1396 (2008)], we present here a systematic investigation of this phenomenon, considering a short, an intermediate, and a large shoulder width. © *2008 American Institute of Physics*. [DOI: 10.1063/1.3006065]

I. INTRODUCTION

For more than 25 years considerable effort has been dedicated to study the thermodynamic, structural, and dynamical properties of hard core particles with an adjacent soft repulsive shoulder, i.e., so-called core softened potentials. This class of potentials was probably first considered by Hemmer and Stell[1] in 1970 in a model where the soft repulsion was characterized by a linear ramp with an additional, weak attractive tail. The system was introduced in an effort to study the possibility of the occurrence of more than one critical point in the phase diagram of a simple model system. In numerous, subsequent investigations evidence was provided for a surprisingly rich variety of rather unusual properties of this class of systems: these features range from isostructural solid-solid transitions, where possibly several solid structures are involved (see, e.g., Refs. 2–7), over a very complex phase diagram of the solid phases,[8,9] to different sorts of anomalous behavior, encountered in the static and/or in the dynamic properties (see, e.g., Refs. 10–14).

Within this class of core softened potentials the square-shoulder interaction, consisting of an impenetrable hard core with an adjacent, repulsive shoulder (or corona), is undoubtedly the simplest representative. Despite its simple, radially symmetric functional form this system is nevertheless able to offer a large variety of unexpected features, which are mostly related to its structural properties. This propensity and ability for unconventional self-assembly scenarios was already discovered in the remarkable study by Jagla[9] on a particular family of *two*-dimensional core softened systems, where the square-shoulder system was included as a special case: in this contribution evidence was given that the particles are able to self-organize in a surprisingly broad variety of highly complex ordered structures. In subsequent work on the two-dimensional case these particle arrangements that include, among others, cage or lane formation as well as micellar or inverse micellar configurations were confirmed or newly discovered both in computer simulations[15,16] and in theoretical investigations.[17] A more systematic study of the ordered particle configurations of the two-dimensional square-shoulder system was presented in Ref. 18.

The aim of the present contribution is to investigate in a systematic and thorough way the ordered particle arrangements of the square-shoulder system in *three* dimensions. To this end we study the system at $T=0$ and in the NPT ensemble; thus, we search for configurations that minimize the Gibbs free energy, which we will term—to be consistent with previous contributions—as minimum energy configurations (MECs). To provide a deeper insight into the self-assembly strategies of the system, we have considered a small, an intermediate, and a large shoulder range. While preliminary results have already been presented in Ref. 19, we identify in the present, more systematic investigation an overwhelmingly rich variety of MECs. Analyzing these data, we give evidence that these MECs can be grouped together in four structural archetypes that emerge in dependence of the value of the pressure P that is exerted on the system: *cluster* structures are preferentially formed at low P values, while *columnar* and *lamellar* structures are predominantly identified at intermediate pressure values; finally, *compact* particle configurations emerge at high pressures. While this general rule might still be less obvious at small shoulder range, it is nearly perfectly obeyed for an intermediate shoulder width and definitely holds for the case of a broad corona. With its simple functional form the interparticle interaction offers not only many computational advantages.[20] It allows to *understand* via simple geometrical considerations the system's self-assembly strategy: it is, in particular, the range of the

[a]Electronic mail: pauschenwein@cmt.tuwien.ac.at.

shoulder that turns out to be responsible in a highly sophisticated way for the formation of the complex structures. In addition, the flat energetic plateau of the shoulder with its finite range represents a very sensitive antenna to distinguish between energetically competing structures. Our observations provide a deeper insight into the system's strategy to form ordered equilibrium particle configurations, a knowledge that might be useful to understand self-assembly processes in other systems with more complex interactions.

Objections against the simple functional form of the potential are refuted by the argument that it is able to capture the essential features of colloidal particles with core-corona architecture as they are, for instance, treated in Ref. 21 and references therein. Indeed, several of the MECs that we could identify had already been encountered in previous theoretical, experimental, and computer simulation investigations: micellar and inverse micellar structures,[17,22] spirals,[23] chains and layers,[8,9,11,17,24,25] and cluster phases,[26–28] to name a few examples.

Although the identification of MECs represents a "simple" optimization problem of the Gibbs free energy, its solution has turned out to be highly nontrivial. In this contribution we present a systematic sequence of ordered MECs for the three selected values of shoulder width. This achievement is mainly due to our search strategy, which is based on ideas of genetic algorithms (GAs). Introduced already several decades ago in a completely different context,[29] these approaches have meanwhile become a highly appreciated optimization tool to identify ordered particle arrangements both in hard[30–32] as well as in soft matter systems.[18,19,33–36] The high reliability, flexibility, and efficiency of GA-based optimization strategies, in combination with a particular search strategy that is intimately related to the simple functional form of the square-shoulder potential, make us believe that the sequences of MECs that will be presented and discussed in the following are complete.

The paper is organized as follows. In Sec. II we briefly present the square-shoulder system. Section III deals with the theoretical tools of this contribution: the GA-based search strategy as well as the theoretical considerations to identify close-packed particle arrangements of the system as a function of the shoulder width. The results of our investigations are summarized in Sec. IV: we start with the close-packed particle arrangements (as they play a key role in the search strategy) and present and discuss in the following the MECs that we have identified for the three different cases of shoulder width. The conclusions of the contribution are summarized in Sec. V, which also contains the discussion of possible future work.

II. MODEL

We consider a system of particles that interact via the square-shoulder potential, which we parametrize as follows:

$$\Phi(r) = \begin{cases} \infty, & r \leq \sigma, \\ \epsilon, & \sigma < r \leq \lambda\sigma, \\ 0, & \lambda\sigma < r. \end{cases} \quad (1)$$

σ is the diameter of the impenetrable core and $\lambda\sigma$ is the width of the adjacent, repulsive shoulder (or corona) of height ϵ, $\epsilon > 0$. Further, we introduce the number density $\rho = N/V$ (N being the number of particles and V being the volume of the system) and the dimensionless number density $\rho^\star = \rho\sigma^3$. Thermodynamic quantities will be used in the following reduced units: pressure $P^\star = P\sigma^3/\epsilon$, internal energy $e^\star = E/N\epsilon$, and Gibbs free energy $g^\star = G/N\epsilon$. Since we perform our investigations at $T=0$, $G=E+PV$ and hence $g^\star = e^\star + P^\star/\rho^\star$.

The simple functional form of the square-shoulder potential with its constant potential barrier and its finite range makes the system the "quintessential test system"[20] for the purpose of the present contribution. It also simplifies considerably thermodynamic considerations. For a given periodic particle arrangement, which we characterize by the number of overlapping coronas, $e^\star$ is a rational number: it is given as the ratio of the number of overlaps per particle in the unit cell divided by the number of these particles, which we denote as n_b. For this particle arrangement $g^\star = e^\star + P^\star/\rho^\star$ is therefore a linear function of the pressure $P^\star$, and is consequently represented in the $(g^\star, P^\star)$ plane by a straight line: its slope is given by $1/\rho^\star$, while its intercept is the energy of the configuration, $e^\star$. The limiting particle arrangement at low pressures is easily identified as a close-packed arrangement of spheres with diameter $\lambda\sigma$: thus $e^\star = 0$ and the slope of $g^\star$ in the $(g^\star, P^\star)$ diagram is given by $1/\rho^\star_{\min} = \lambda^3/\sqrt{2}$. For the high pressure limit the situation is more delicate: while the slope of $g^\star$ as a function of $P^\star$ is easily identified for obvious reasons as $1/\rho^\star_{\max} = 1/\sqrt{2}$, the value of $e^\star$ depends in a sensitive way on λ. In Sec. III B we will give evidence that the square-shoulder system shows a rich variety of close-packed scenarios as λ varies.

With the above considerations in mind, we can anticipate that the $g^\star$ values of all MECs will be located on a sequence of intersecting straight lines in the $(g^\star, P^\star)$ plane, each of them being characterized by a slope of $1/\rho^\star$, with $1/\rho^\star_{\min} > 1/\rho^\star > 1/\rho^\star_{\max}$, and by an intercept $e^\star$. This fact will simplify considerably our search for MECs (see discussion in Sec. IV B).

III. THEORY

A. Genetic algorithms

The MECs of our system have been identified with a search strategy that is based on ideas of GAs. GAs are very general optimization tools that model natural evolution processes, such as recombination, mutation, or survival of the fittest.[29] Their successful applications in a wide range of fields demonstrate their flexibility and reliability. The basic ideas of GAs can be summarized as follows: the central quantity of this concept is an individual $\mathcal{I}$, which represents a possible solution to the problem. The quality of a solution, i.e., of an individual $\mathcal{I}$, is measured via a so-called fitness function $f(\mathcal{I})$. Individuals with a higher fitness value are as-

sumed to be of higher quality. In our search for ordered particle configurations that minimize the Gibbs free energy, an individual corresponds to a lattice while the fitness function is related to G and will be specified below. Starting from a large number of individuals, which represent the initial generation, individuals of a subsequent generation are created with recombination and mutation processes, both of them having a highly stochastic character. Individuals with a higher fitness value are preferred in the reproduction process. In addition, mutation operations are performed on the individuals with some probability p_m. By iterating this process we create a reasonably large number of generations. The final result of the GA-based search strategy is the individual with the overall highest fitness value.

For our particular problem an individual $\mathcal{I}$ is identified by a (possibly nonsimple) periodic crystal structure. Due to the highly stochastic character of the reproduction and of the mutation processes, a straightforward implementation of the algorithm is prone to propose a large number of ordered configurations where the hard cores of the particles overlap and which therefore correspond to unphysical particle arrangements. This, in turn, causes a drastic reduction in the efficiency of the algorithms. To overcome this problem we have developed a particular parametrization of an *arbitrary* simple lattice via three lattice vectors $\{\mathbf{a}_1,\mathbf{a}_2,\mathbf{a}_3\}$:[37] here, $a_1=|\mathbf{a}_1|$ represents the shortest possible distance between two lattice sites in the entire lattice and $a_2=|\mathbf{a}_2|$ is the second smallest distance in the lattice (i.e., $a_1 \leq a_2$) with $\mathbf{a}_1$ and $\mathbf{a}_2$ being linearly independent; finally, a similar relation holds between $\mathbf{a}_3$ on one side and $\mathbf{a}_1$ and $\mathbf{a}_2$ on the other side. Thus if $a_1 > \sigma$, it is guaranteed that the hard cores of the particles will not overlap and consequently the GA will create only simple lattices where overlap of the cores is avoided *a priori*. For nonsimple lattices, the distances between all particles within the unit cell and including also the particles of the 26 neighboring cells have to be determined. If the smallest of these distances, l_0, is smaller than a_1, then the lattice is scaled with a factor a_1/l_0. The rather complex formalism is most conveniently implemented in the *NPT* ensemble. Thus, a state is characterized by a value for the pressure P, while the equilibrium density ρ is a result of the optimization procedure. For details we refer to Ref. 37.

For the implementation of the individuals we use the encoding strategy for three-dimensional lattices presented in Ref. 35. Note that for each GA run, the number of particles per unit cell has to be fixed; in an effort to identify also complex structures with a large number of basis particles, a series of GA searches has to be performed at each state point where the number of particles per unit cell varies over a reasonable range. Distances and angles are encoded in binary strings with a length ranging from 4 to 6. Since in the *NPT* ensemble the Gibbs free energy has to be minimized, we use the following fitness function:

$$f(\mathcal{I}) = \exp\{-[G(\mathcal{I}) - G(\mathcal{I}_0)]/G(\mathcal{I}_0)\}, \tag{2}$$

where $\mathcal{I}_0$ corresponds to some reference structure. A pool of 700 individuals is evolved through reproduction and mutation processes over 500 generations (for further details concerning these processes, see Ref. 35): creation of individuals of the new generation from individuals of the preceding generation is carried out via one-point or random crossover operations, while the mutation process, which reintroduces lost genetic materials and avoids inbreeding, is realized with a mutation probability of $p_m=5\%$. For each state point, 1000 of such independent runs have been carried out. Finally, the individual with the overall lowest G value, $\mathcal{I}_{\min}$, is considered to be the solution of the GA. To account for the limited accuracy caused by the encoding procedure, the parameters of $\mathcal{I}_{\min}$ were refined via a final Powell optimization algorithm.[38]

B. Close-packed structures

The limiting case at high pressures is always a crystal where the hard cores of the particles arrange in a close-packed structure. Thus the slope of the line that expresses the linear dependence of $g^\star$ on $P^\star$ in the $(g^\star,P^\star)$ plane is obviously given by $1/\rho^\star_{\max}=1/\sqrt{2}$. However, the intercept of this line, i.e., the energy of this arrangement, $e^\star$, requires more careful considerations. Below we will give evidence that the square-shoulder system is able to self-organize not only in the well-known close-packed scenarios, i.e., in fcc or hexagonally close-packed (hcp) lattices, but also in more complex structures.[39] We emphasize that the square-shoulder system serves—due to its flat plateau and due to the finite range of the corona—as an antenna that is able to identify in a very sensitive way between competing particle arrangements.

In an effort to find for a given value of λ the energetically most favorable close-packed arrangement of the particles, we proceed as follows. We consider the lattice as being built up by periodically repeated stacking sequences of n_l hcp layers, introducing for convenience the conventional labels, A, B, and C.[40] A stacking sequence of n_l layers can therefore be described by a string of n_l of these symbols. The trivial close-packed arrangements, fcc and hcp, are thus characterized by the sequences ABC (with $n_l=3$) and AB (with $n_l=2$). For a given value of n_l we consider all possible stacking sequences of length n_l; without loss of generality we start all sequences with the label A. Some of the proposed sequences *have* to be ruled out: this is the case when two neighboring layers carry the same index. Some of them *can* be ruled out: this is, for instance, the case when symmetry considerations reveal that two different stacking sequences lead to the same crystal.

Pursuing this strategy we find for the smallest n_l values the following situation: for $n_l=2$ we have only the hcp structure (AB) and for $n_l=3$ we recover the fcc lattice (ABC). Also for four- and five-layer stackings only one representative remains: $ABAC$ and $ABABC$ can be identified, respectively. At $n_l=6$, we encounter for the first time two nonequivalent stacking sequences, namely, $ABABAC$ and $ABACBC$. With increasing n_l the number of possible stacking sequences increases drastically. For instance, for $\lambda=4.5$, where we have considered stackings with up to 12 layers, we were able to identify 133 different sequences. A comprehensive table of possible stacking sequences for a given value of n_l is presented in Ref. 41.

Finally, for a given value of λ we include a sufficiently

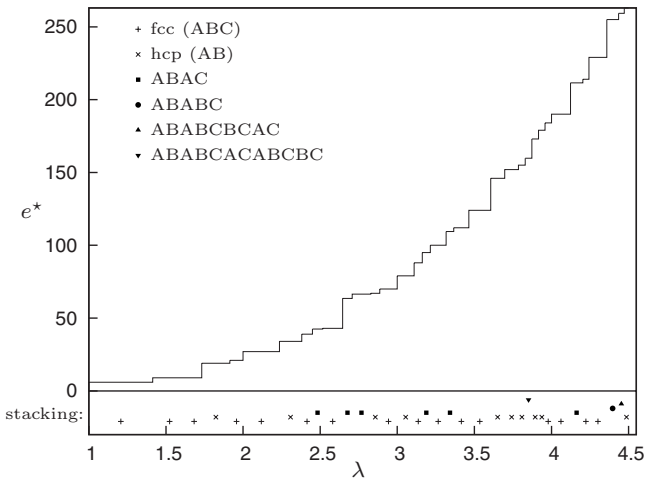

FIG. 1. Energy per particle, $e^\star$, for the simplest, energetically most favorable close-packed particle arrangements for the square-shoulder system as a function of λ (full curve). Symbols specify the stacking sequences as labeled; see also text.

large number of layers and evaluate and compare the energies $e^\star$ of all candidate stackings. The finite range of the shoulder and its flat energy plateau help reduce the numerical effort considerably. On some occasions we encounter degeneracy, i.e., two (or even more) different stacking sequences are characterized by exactly the same value of $e^\star$. In such cases, we consider the shortest among these stacking sequences to be the energetically most favorable configuration with the only exception that we favor fcc to hcp.[42]

IV. RESULTS

A. Close-packed structures

With the above considerations in mind we can now identify the equilibrium close-packed structures for the square-shoulder system as they occur at high pressure values. These particle arrangements are summarized in Fig. 1, starting from $\lambda=1$ (corresponding to hard spheres) and extending to a shoulder width of $\lambda=4.5$. The figure contains the energy $e^\star$ of the respective structures and symbols characterize their stacking sequences.

As long as $1<\lambda<\sqrt{2}$, only nearest neighbor interactions have to be considered. All stackings are characterized by the same number of overlapping coronas; the energy of a tagged particle amounts to half the number of nearest neighbors, i.e., $e^\star=6$. Although for $\sqrt{2}<\lambda<2\sqrt{2/3}$, the second nearest neighbors start to play a role, we still obtain for all possible stackings the same value for $e^\star$, namely, $e^\star=9$. For $2\sqrt{2/3}<\lambda<\sqrt{3}$, the different stackings are characterized by different energy values; among these, the fcc structure is one of the stackings with the lowest $e^\star$ value, namely, $e^\star=9$, while all other stackings are energetically equal or less favorable. Therefore in this λ interval, fcc remains the simplest, energetically most favorable structure. For $\lambda=\sqrt{3}$, a hcp lattice with $e^\star=19$ becomes the simplest structure with the lowest e value. Further stacking sequences can be extracted from Fig. 1 for λ values up to 4.5. This figure shows that for a few λ intervals also stacking sequences other than fcc or hcp are obtained as the energetically most favorable close-packed particle arrangements at high pressures.

TABLE I. Standard abbreviations for the 14 Bravais lattices used in the text and the captions. The seven crystal systems are separated by blank rows.

Bravais lattice	Abbreviation
Simple cubic	sc
Body centered cubic	bcc
Face centered cubic	fcc
Hexagonal	hex
Trigonal (rhombohedral)	trig
Simple tetragonal	st
Centered tetragonal	ct
Simple orthorhombic	so
Single face centered orthorhombic	sfco
Body centered orthorhombic	bco
Face centered orthorhombic	fco
Simple monoclinic	sm
Single face centered monoclinic	sfcm
Triclinic	tric

B. Configurations that minimize the Gibbs free energy

Once we have determined the limiting high pressure MECs, we can proceed to the identification of the whole sequence of MECs as a function of the pressure. This is done in Secs. IV B 1–IV B 3 where we have considered square-shoulder systems with a short ($\lambda=1.5$), an intermediate ($\lambda=4.5$), and a large ($\lambda=10$) shoulder width. Abbreviations of the underlying lattices that are used in the text and in the figures are summarized in Table I.

For $\lambda=1.5$ we shall give a detailed geometrical interpretation of these particle arrangements; this will provide clear evidence about the system's strategy to arrange the particles at a given pressure in such a way as to minimize the number of overlapping shoulders and to maximize at the same time the density. Although we will not be able to pursue these geometrical considerations in full detail for the other λ values, we will be able to identify an emerging sequence of structural archetypes as we increase the pressure: while at low pressures particles tend to arrange in clusters, which then populate the positions of regular lattices, we encounter with increasing pressure columnar, lamellar, and, finally, compact structures. With a few exceptions this rule is obeyed for $\lambda=4.5$, while it is strictly followed for $\lambda=10$. For a more detailed presentation we refer to Ref. 41.

Before we present and discuss the sequences of MECs in detail we briefly outline how we can take benefit from the fact that for this particular system $g^\star$ is a linear function of $P^\star$. Our search algorithm is sketched in Fig. 2. In the first step, we determine the intersection point of the two straight

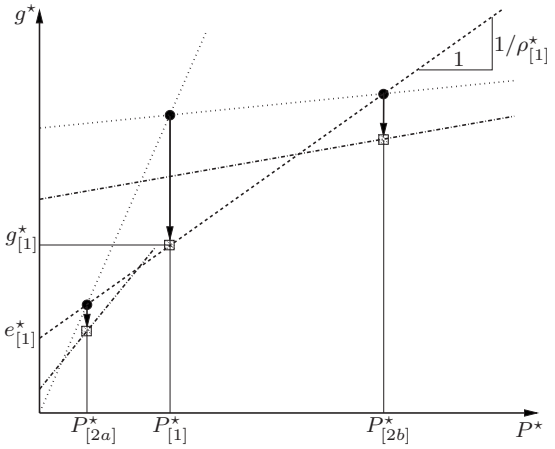

FIG. 2. Schematic of our search strategy to identify MECs in the $(g^\star, P^\star)$ plane. The dotted lines represent $g^\star$ as a function of $P^\star$ for the limiting low and high pressure configurations: The vertical arrows represent GA runs that identify, starting from an initial guess (dot), an energetically more favorable MEC (square). For details see text.

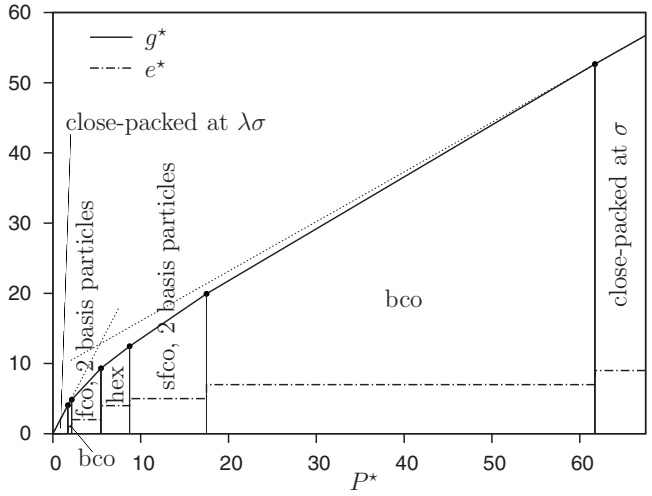

FIG. 3. $g^\star$ and $e^\star$ as functions of $P^\star$ for the ordered equilibrium structures identified for the square-shoulder system with $\lambda=1.5$, as labeled. The dotted lines indicate the low and high pressure limiting configurations (see text). The identified lattices are indicated by standard abbreviations (see Table I), including, if required, the number of basis particles; see also Fig. 4.

lines in the $(g^\star, P^\star)$ diagram which represent the high and the low pressure limiting cases; let the corresponding pressure value be $P^\star_{[1]}$. At this state point we perform a sequence of GA searches. In each of these runs we consider a different number of basis atoms, where the maximum number of basis particles depends on the value of λ. This optimization step leads to a new particle configuration which is characterized by a Gibbs free energy $g^\star_{[1]}$ that is lower than the one of the intersection point, by a density $\rho^\star_{[1]}$, and by an energy $e^\star_{[1]}$. Thus this particle arrangement is at given pressure $P^\star_{[1]}$ the energetically most favorable one. $e^\star_{[1]}$ and $\rho^\star_{[1]}$ define a new line in the $(g^\star, P^\star)$ plane; we determine the two intersection points of this line with the two lines representing the limiting configurations leading to the pressure values $P^\star_{[2a]}$ and $P^\star_{[2b]}$. At these two state points we launch new GA searches. This procedure is repeated until at none of the intersection points of an iteration step an energetically more favorable particle arrangement can be identified. On one side this procedure avoids a rather time-consuming scan of the pressure range on a finite grid and thus brings along a considerable reduction in the number of GA steps and, consequently, of the computational effort; on the other side this strategy avoids the risk of simply "forgetting" MECs. Both features become more and more important with increasing shoulder width since the distribution of MECs over the whole pressure range is highly nonlinear, as can be seen in Figs. 3, 5, and 7.

This systematic search strategy, in combination with the reliability of GA-based optimizations, makes us confident that the sequences of MECs that we shall present in the following are complete.

1. Short shoulder width ($\lambda=1.5$)

The phase diagram (i.e., $g^\star$ and $e^\star$ as functions of $P^\star$) for the square-shoulder system with $\lambda=1.5$ is depicted in Fig. 3; the corresponding ordered equilibrium structures are compiled in Fig. 4, except for the trivial low and high pressure structures, where particles arrange in any close-packed crystal structure, which we take to be fcc (see discussion above). Further numerical details about the seven identified MECs are compiled in Table II. Although we have considered in our search strategy crystals with up to eight basis particles, only crystals with at most two basis particles were identified. The limiting low pressure configuration is characterized by $e^\star=0$ and $\rho^\star=\sqrt{2}/\lambda^3\simeq 0.629$. Further, since $\lambda=1.5$ is slightly larger than $\sqrt{2}$, we are above the threshold value (see discussion in Sec. IV A) where the hard cores of the particles form a close-packed structure and only the coronas of nearest neighboring particles overlap; thus $e^\star=9$ and $\rho^\star=\sqrt{2}$.

As we start our search in the low pressure regime, the first nontrivial structure we encounter is a body centered orthorhombic (bco) structure [Fig. 4(1)]. A more detailed consideration identifies this particle arrangement as a columnar structure: particles form lanes along which the hard cores are in direct contact. While, of course, these lanes lead to an intracolumnar shoulder overlap along the lanes, any other intercolumnar overlap is avoided; consequently, $e^\star=1$. Simple geometric considerations reveal that the edge lengths of the conventional bco unit cell have the following values: σ, $\lambda\sigma$, and $\sqrt{3\lambda^2-1}\sigma$.

The avoidance of intercolumnar shoulder overlap has to be sacrificed as the pressure is further increased, leading to a rather compact structure: we identify a face centered orthorhombic lattice with an additional basis particle (color code: blue) [see Fig. 4(2)]. This particle is in direct hard core contact with its four nearest neighbors: three of them are located at the faces (color code: red) and one sits at the corner (color code: green) of the conventional unit cell. Furthermore, this particle is separated by a distance $\lambda\sigma$ from its second nearest neighbor (color code: green) which occupies another corner of the conventional orthorhombic unit cell. Finally, particles at the smallest faces of the cell (color code: red) are positioned in such a way that their shoulders touch the shoulders of the particles located at the corners of the corresponding face of the conventional orthorhombic unit cell (color code:

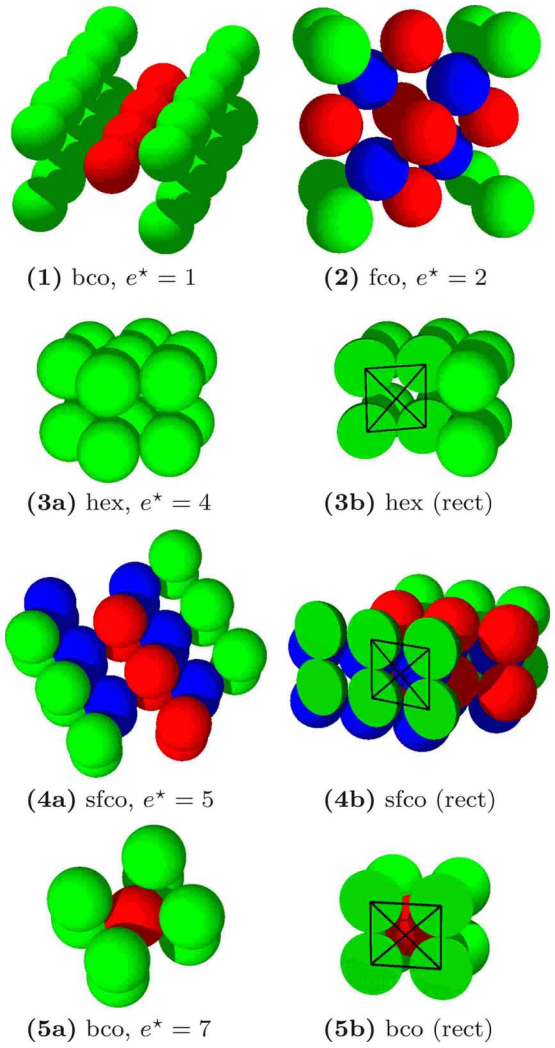

FIG. 4. (Color online) Visualization of the nontrivial ordered equilibrium structures for the square-shoulder system with $\lambda = 1.5$. Structures are characterized by standard abbreviations (see Table I) and their respective $e^\star$ value. Grayscale (color) code: light (green), articles at the corner positions of the conventional unit cell; medium (red), particles at body or face centered positions; dark (blue), additional basis particles.

TABLE II. Numerical details of the ordered equilibrium structures identified for the square-shoulder system with $\lambda = 1.5$: the underlying lattice is characterized by the according abbreviation (see Table I). n_b is the number of basis particles required to describe the MEC. $e^\star$ and $\rho^\star$ are the energy per particle and particle density, respectively. Since the MECs can be interpreted on the basis of geometric considerations, $\rho^\star$ can be given in closed, analytic expressions.

Lattice	n_b	$e^\star$	$\rho^\star$
fcc	1	0	$8\sqrt{2}/27 \simeq 0.419$
bco	1	1	$8/3\sqrt{23} \simeq 0.556$
fco	2	2	$16/\sqrt{455} \simeq 0.750$
hex	1	4	$4/\sqrt{15} \simeq 1.03$
sfco	2	5	$16/2\sqrt{15}+\sqrt{35} \simeq 1.17$
bco	1	7	$8/\sqrt{35} \simeq 1.35$
fcc	1	9	$\sqrt{2} \simeq 1.41$

green). These considerations fix the edge lengths of the unit cell to be $\sqrt{2\lambda^2-2}\sigma$, $\sqrt{2\lambda^2+2}\sigma$, and $2\sqrt{4-\lambda^2}\sigma$.

As we further increase the pressure the particles arrange in a MEC that can be identified as a lamellar structure, see Fig. 4(3a). It can be described as a stacking of hcp layers which are placed exactly on top of each other. The nearest neighbor distance is obviously σ. The second nearest neighbors are separated by the interlayer distance which is fixed by the requirement that the corona of a tagged particle touches the shoulders of its 12 third nearest neighbors, located in the adjacent layers. Thus, this distance amounts to $\sqrt{\lambda^2-1}\sigma \sim 1.12\sigma$. It should be pointed out that particles in nearest and second nearest neighbor distances form a rectangular particle arrangement [emphasized in Fig. 4(3b)] that will also be encountered in the subsequent MECs: if we consider within a layer two particles in close contact, then they form with the corresponding particles of one of the adjacent layers a rectangle with edge lengths σ and $\sqrt{\lambda^2-1}\sigma$.

For even higher pressure values only compact structures are identified. The next MEC can be described as a single face centered orthorhombic lattice with two basis particles, visualized in Fig. 4(4a). The orthorhombic unit cell is built up by two side faces that have exactly the aforementioned rectangular shape [formed by particles in green, emphasized in Fig. 4(4b)], while the two larger side faces are each decorated in their center by an additional particle (color code: red). Finally, the additional basis particles (color code: blue) are located in such a way that they are in direct contact both with the four particles forming the side faces as well as with the two red particles located in the other side faces. Simple geometric considerations lead to the edge lengths of the orthorhombic cell, namely: σ, $\sqrt{\lambda^2-1}\sigma$, and $(\sqrt{3}+\sqrt{4-\lambda^2})\sigma$.

The last nontrivial compact structure is a bco lattice [emphasized in Fig. 4(5a)]. Again, we can easily identify the side faces of the conventional unit cell as the above mentioned rectangular structure [see Fig. 4(5b)]. In addition, the central particle is in direct hard core contact with the particles forming the unit cell. Based on these geometrical considerations the edge lengths of the unit cell can easily be identified to be σ, $\sqrt{\lambda^2-1}\sigma$, and $\sqrt{4-\lambda^2}\sigma$.

2. Intermediate shoulder width ($\lambda = 4.5$)

A much larger diversity in the ordered equilibrium structures could be identified for an intermediate shoulder width of $\lambda = 4.5$. The limiting low pressure MEC is of course again a fcc structure with a nearest neighbor distance $\lambda\sigma$ and, hence, $e^\star = 0$. On the other hand, the high-density limiting particle configuration is a hcp lattice with $e^\star = 263$ (see Fig. 1 and discussion in Sec. IV A). With the help of the GA we have obtained in total 33 different MECs over the entire pressure regime. In our investigations unit cells with up to ten basis particles have been considered; in the end only configurations with up to eight basis particles were part of the MECs.

A first look at these MECs gives evidence that within this sequence of MECs we can easily identify the aforementioned four structural archetypes: at low pressures, the system prefers to form cluster structures; with increasing pres-

TABLE III. Numerical details of the ordered equilibrium structures identified for the square-shoulder system with $\lambda=4.5$: the underlying lattice is characterized by the according abbreviation (see Table I). n_b is the number of basis particles required to describe the MEC. $e^\star$ and $\rho^\star$ are the energy per particle and particle density, respectively. The abbreviation in the third row indicates to which of the four archetypes the MEC belongs (clu, cluster; col, columnar; lam, lamellar; com, compact). Closed, algebraic expressions for $\rho^\star$ can be derived but are not presented here due to space limitations. For details see Ref. 41.

Lattice	n_b	Shape	$e^\star$	$\rho^\star$
fcc	1	clu	0	0.0155
sm	2	clu	1/2	0.0235
sfcm	3	clu	1	0.0291
tric	8	clu (4)	3/2	0.0343
tric	4	clu	7/4	0.0369
tric	6	clu	5/2	0.0454
bco	1	col	3	0.0512
bco	8	clu	35/8	0.0638
tric	2	col	13/2	0.0799
sm	2	col	8	0.0923
tric	2	col	21/2	0.104
bco	1	lam/col	15	0.135
trig	1	lam	18	0.154
tric	2	lam	20	0.168
tric	2	lam (col)	49/2	0.198
trig	2	lam	30	0.243
trig	2	lam	61/2	0.245
ct	2	lam	77/2	0.283
sfcm	2	lam	56	0.383
sm	2	lam	58	0.394
fco	2	lam	143/2	0.484
bcc	1	com	90	0.567
ct	1	com	96	0.594
tric	3	lam	337/3	0.677
trig	1	com	115	0.692
sc	1	com	128	0.763
hex	1	com	138	0.811
bcc	1	com	169	0.997
ct	1	com	180	1.05
sfcm	1	com	210	1.21
fcc	1	com	229	1.29
ct	1	com	243	1.34
hcp	2	com	263	1.41

sure, columnar structures are formed, which then transform into lamellar particle arrangements; finally, at high pressures, we observe compact structures. This rule, which is disobeyed only twice for $\lambda=4.5$, can nicely be understood via a detailed analysis of the particle arrangements, reflecting the system's strategy to reduce at a given pressure the number of overlapping coronas as much as possible (i.e., minimizing $e^\star$) while maximizing at the same time the particle density.

Numerical details about these ordered structures are summarized in Table III. The phase diagram for the square-shoulder system with $\lambda=4.5$ is depicted in Fig. 5. It also contains information to which class of the four archetypes a particular MEC belongs to. Finally, the horizontal bar at the bottom of the figure indicates those MECs where no direct contact between the cores of the particles occurs.

At low pressure values (i.e., up to $P^\star \simeq 0.5$) particles prefer to arrange in ordered clusters of up to eight particles,

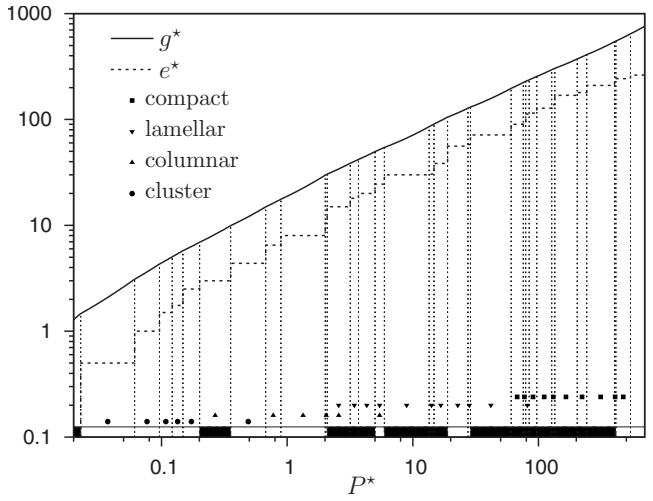

FIG. 5. $g^\star$ and $e^\star$ as functions of $P^\star$ on a double logarithmic scale for the ordered equilibrium structures identified for the square-shoulder system with $\lambda=4.5$, as labeled; note that due to the nonlinear scale, the linear dependence between $g^\star$ and $P^\star$ is no longer visible. The structural archetypes to which a given MEC belongs (cluster, columnar, lamellar, or compact structure) are specified by a symbol (as labeled). The black horizontal bar at the bottom of the figure indicates those ordered particle arrangements where no direct contact between the cores of the particles is observed.

which populate the positions of crystal lattices. A closer analysis of these structures reveals a strong interplay between the shape of the clusters and of the symmetry of the unit cell: the more aspherical the clusters are, the lower is the symmetry of the lattice. This tendency reflects the system's efforts to avoid to the highest possible degree a shoulder overlap of neighboring clusters. A nice visualization of this strategy can, for instance, be observed in the structure depicted in Fig. 6(5): the rather elongated four-particle clusters are located on a low-symmetry triclinic lattice; on the other hand, the nearly spherically shaped eight-particle clusters of the structure depicted in Fig. 6(8) populate the lattice positions of a bco structure, which has a considerably higher symmetry. A systematic, quantitative analysis of all cluster structures reveals that for most of these MECs only rarely are shoulder overlaps of neighboring clusters observed. A nice example that demonstrates the complexity of cluster structures is depicted in Fig. 6(4). In this MEC we can identify two different sorts of clusters: tetrahedral clusters occupy the corners of a triclinic lattice, while the other four-particle cluster species populates a central position in the body of the triclinic cell.

As the pressure is further increased there is a drastic change in the system's strategy to arrange particles, namely, the formation of columnar structures, where particles self-organize in lanes. This leads to a considerable energetic penalty, since—due to the short interparticle distance within the columns—an appreciable number of overlapping shoulders is induced; at the same time a rather high particle density is guaranteed along these lanes which, in turn, contributes to a reduction in the Gibbs free energy. Simultaneously, the system tries to compensate for this high energetic cost within the lanes by arranging these columns in such a way as to minimize the intercolumnar shoulder overlap. This strategy leads first to the formation of single-columnar structures [as

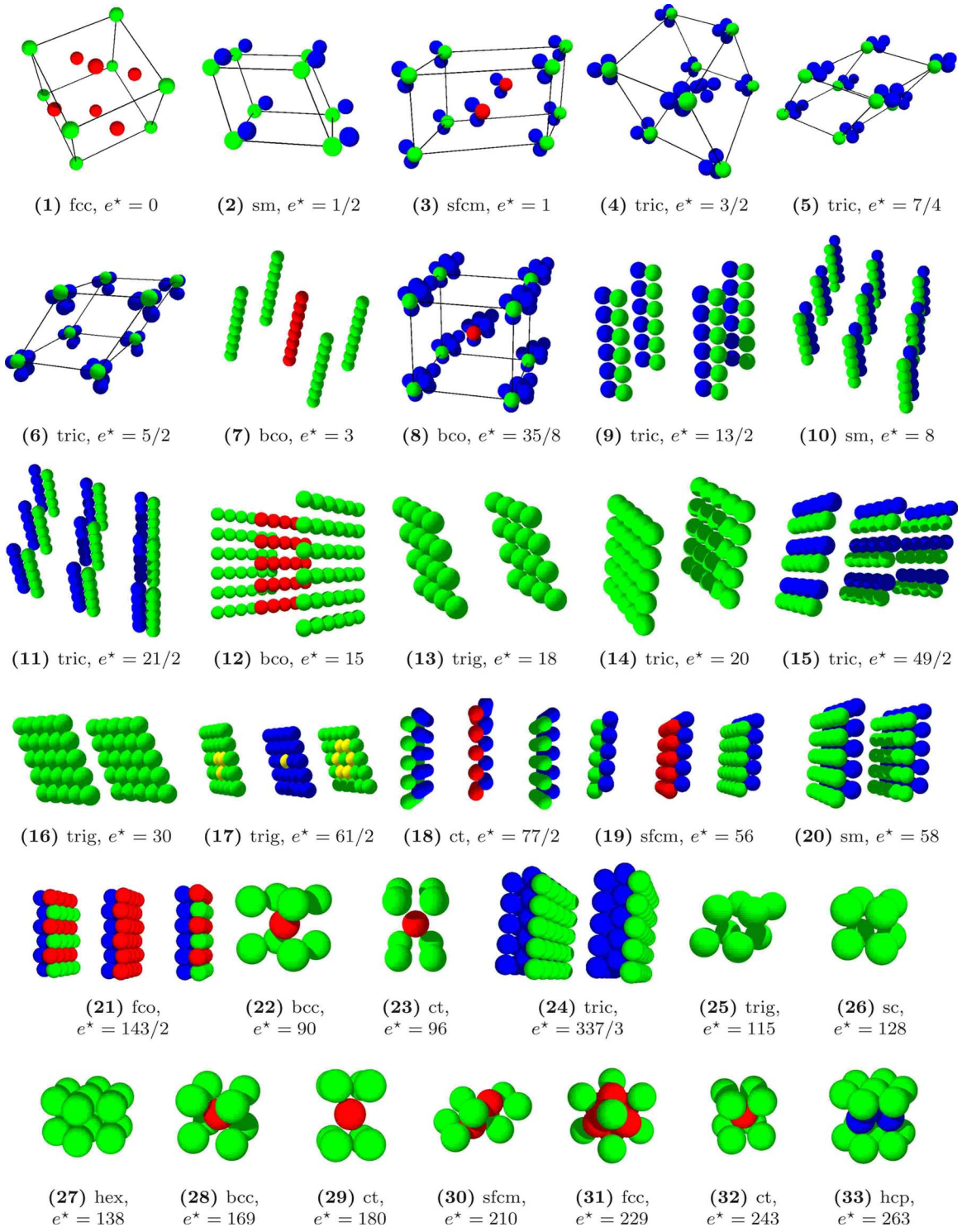

FIG. 6. (Color online) Visualization of all 33 ordered equilibrium structures for the square-shoulder system with $\lambda = 4.5$. Structures are characterized by standard abbreviations (see Table I) and their respective $e^\star$ value. Grayscale (color) code: light (green), particles at the corner positions of the conventional unit cell; medium (red), particles at body or face centered positions; dark (blue), additional basis particles. The shoulders of the very light (yellow) particles in panel (17) touch the ones of the other very light (yellow) particles, located in the neighboring layers.

depicted in Fig. 6(7)], and later, as the pressure is increased, to double-columnar particle arrangements [see Figs. 6(9)–6(11)]. We point out that within the lanes particles are only in direct contact at sufficiently high pressures; in double-columnar structures, particles of adjacent columns are always in direct contact. The system's strategy to avoid shoulder overlap between the lanes can nicely be traced in a closer analysis: for the structures depicted in Figs. 6(7), 6(9), and 6(10), no corona overlap between the single or double strands is observed; only at sufficiently high pressures—see Fig. 6(11)—do the coronas of different neighboring double columns start to overlap.

For pressures values above $P^\star \gtrsim 3$, the system has to search for new ideas of how to minimize the Gibbs free

energy. Now the change to a new strategy is considerably smoother than the preceding one: in an effort to cope with the increasing pressure the system forms lamellar structures—see Figs. 6(12)–6(21) and 6(24). These MECs emerge from columnar structures as the columns approach each other, forming thereby lamellas; some intermediate stages of this transition can be observed in Figs. 6(12) and 6(15). Within the lamellar structure the system's strategy is obvious. First optimize the packing inside a layer, leading to hexagonal particle arrangements inside a lamella: while at low pressure values [Figs. 6(13) and 6(14)] particles are more loosely packed, they are forced to form a nearly hcp structure with a nearest neighbor distance of $\simeq 1.03\sigma$ at higher pressures [Figs. 6(16) and 6(17)]. Particular attention should be dedicated to the latter structure: the three neighboring, parallel planes depicted in Fig. 6(17) are *not* equally spaced; the two different emerging interlamellar distances are rather governed by the fact that the shoulders of the particles marked in yellow located in the three neighboring layers touch. If the possibility for optimizing the packing within a single lamella has been exhausted, the system starts to form double layers [see Figs. 6(18)–6(21)] or even triple layers [see Fig. 6(24)]. A closer analysis of the double-layer structure reveals a very complex strategy which we try to explain as follows. We consider two pairs of neighboring double layers. On one hand we observe shoulder overlap between single layers (belonging to different pairs) that face each other: for instance, in Fig. 6(19), the layer formed by blue particles in the leftmost layer pair and the layer formed by red particles in the central layer pair; on the other hand the distance between pairs of layers is chosen in such a way as to avoid shoulder overlap of single layers that do not face each other: for example, in Fig. 6(19), the layers formed by green particles and the layers formed by red particles. These observations turn out to be valid for all double-layer structures that have been identified for this particular shoulder width.

Finally, we enter for high pressure values the regime of compact structures, characterized, in general, by a large number of nearest neighbors. In most of these MECs direct core contact is avoided (see horizontal bar in Fig. 5), only in the high pressure regime, where a centered tetragonal lattice [see Fig. 6(32)] and, finally, a hcp structure [the limiting case for $\lambda=4.5$, see Fig. 6(33)] are the respective MECs, the cores are in direct contact. Again, with simple geometric considerations, the system's strategy to form MECs can be traced back to avoiding unnecessary shoulder overlap while maximizing the particle density.

3. Large shoulder width ($\lambda=10$)

Finally, we consider the case of a large shoulder width for which we have chosen $\lambda=10$. Now the hard core region is relatively small with respect to the shoulder range. Thus at low densities the core plays a minor role and the system becomes closely related to the penetrable sphere model (PSM).[43] The PSM belongs to a class of soft matter systems where particles are able to solidify in so-called cluster phases,[44] i.e., where particles form stable clusters which populate the positions of periodic lattices. Evidence for this particular phase behavior has been given in density functional based investigations and in computer simulations for the PSM (Ref. 45) and via purely theoretical considerations, combined with computer simulations for a closely related model potential.[27,28,46,47] As we will show below, such cluster phases can also be observed for the square-shoulder system at low pressure values where the hard cores of the particles still have a negligible effect on the properties of the system.

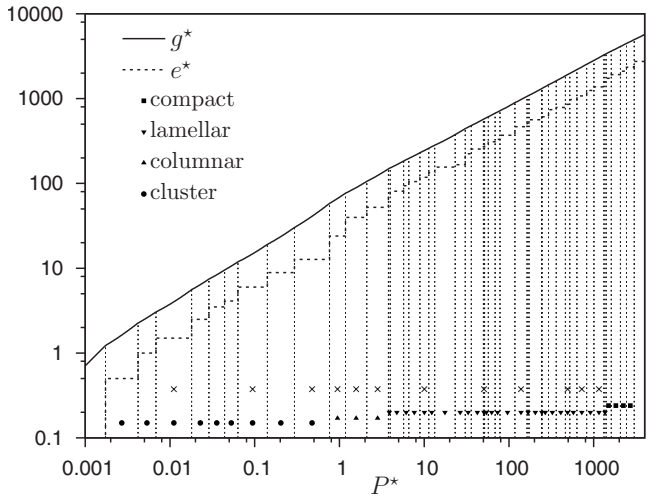

FIG. 7. $g^\star$ and $e^\star$ as functions of $P^\star$ on a double logarithmic scale for the ordered equilibrium structures identified for the square-shoulder system with $\lambda=10$, as labeled; note that due to the nonlinear scale, the linear dependence between $g^\star$ and $P^\star$ is no longer visible. The structural archetypes to which a given MEC belongs (cluster, columnar, lamellar, or compact structure) are specified by a symbol (as labeled). Ordered equilibrium structures marked by crosses are visualized in Fig. 8.

Since the MECs are expected to be rather complex we have considered up to 29 basis particles in our GA-based search strategy; up to 22 appeared in the MECs. In total we have identified as much as 47 MECs, i.e., a relatively large number which makes detailed discussion and interpretation of the structures impossible. The thermodynamic properties of all these MECs are displayed in Fig. 7. We point out that the high pressure limiting configuration is a fcc lattice with $e^\star=2947$. For the case $\lambda=10$ the rule for the sequence of structural archetypes (cluster-columnar-lamellar-compact structures) is strictly obeyed (see symbols in Fig. 7).

As expected cluster structures emerge at low pressure values. A few examples of the ten cluster structures that have been identified are depicted in Figs. 8(1)–8(3). The clusters can contain as many as 22 particles [e.g., in the structure depicted in Fig. 8(3)] and are arranged in complex structures. An example for a typical cluster is depicted in Fig. 8(2); in general the intracluster arrangement of the particles turns out to be irregular.

At $P^\star\simeq 0.76$ the transition to the columnar structures occurs. The relatively large shoulder width allows for a large variety of columnar morphologies, including multicolumnar arrangements or complex helical columns—see Figs. 8(4)–8(6). In Fig. 8(5) a side view of a single column gives evidence of its complex internal structure. Ten basis particles were required to parametrize this MEC; a single column can be considered to be built up by a sequence of aligned clusters. We point out that also in experiment helical columns were observed for a particular class of colloidal particles.[23]

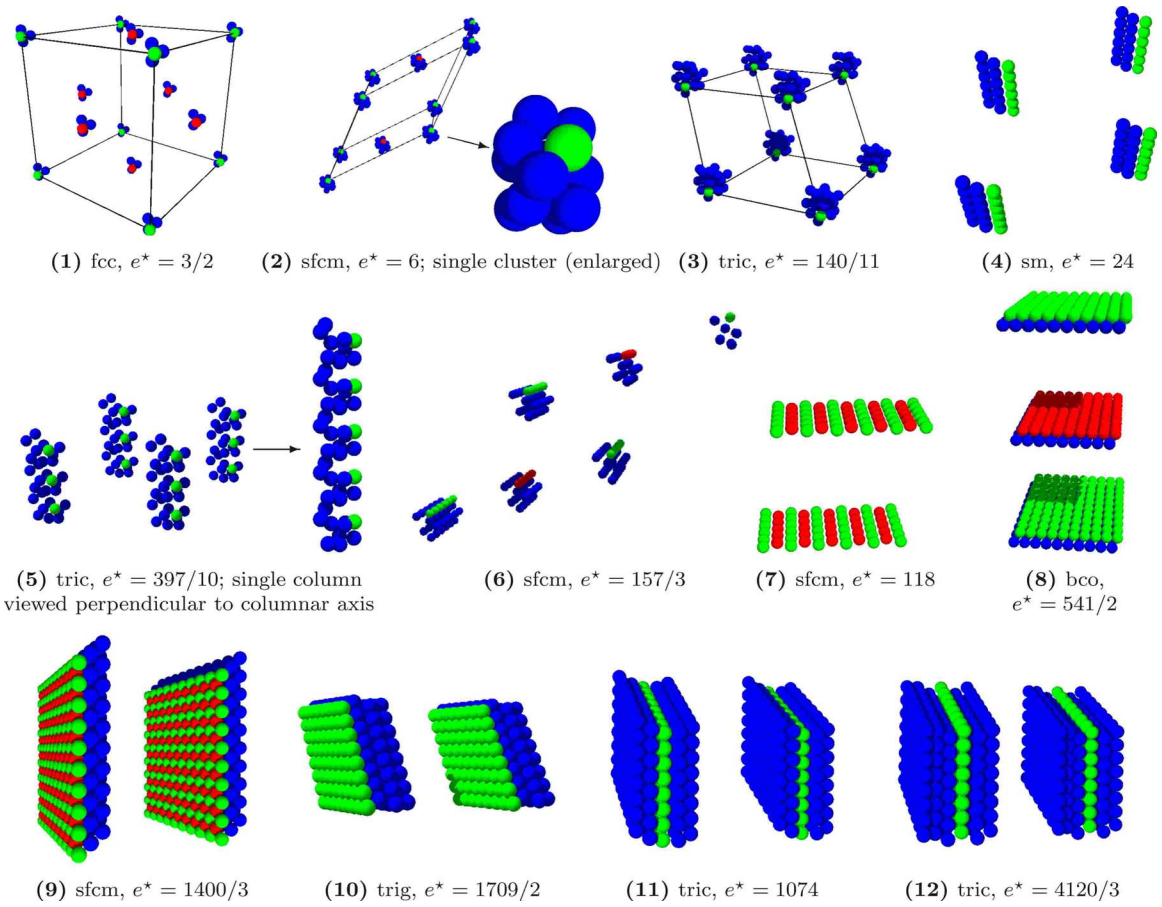

FIG. 8. (Color online) Visualization of a selection of the 47 ordered equilibrium structures for the square-shoulder system with $\lambda=10$. Structures are characterized by standard abbreviations (see Table I) and their respective $e^\star$ value. Grayscale (color) code: light (green), particles at the corner positions of the conventional unit cell; medium (red), particles at body or face centered positions; dark (blue), additional basis particles.

Examples for multicolumnar arrangements are the triple columns displayed in Fig. 8(4) or the MEC shown in Fig. 8(6): here six parallel single columns that are nearly in close contact are aligned in parallel to build the sixfold column, as can be seen from the rightmost column, where the direction of projection has been chosen to be parallel to the columnar axis.

Most of the MECs identified for the case $\lambda=10$ have lamellar character: in total we have identified as much as 28 lamellar MECs. Again, we observe a similar strategy as the one identified for $\lambda=4.5$: first the particle arrangement within the single layer structures is optimized; then, if this possibility for close-packed arrangements is exhausted, multilayer structures are formed. The large shoulder width is responsible both for the large interlayer distance as well as for the close contact within groups of lamellas: One has the impression that the large range of the shoulder compactifies adjacent layers, bringing them in direct contact, while maximizing at the same time the distance between these groups of layers [see Figs. 8(8)–8(12)].

Finally, we enter the regime of compact structures. Since they resemble very closely those MECs that have been identified for $\lambda=4.5$, we do not present them here.

V. CONCLUSIONS

In this contribution we have thoroughly investigated the phase diagram of the square-shoulder system at $T=0$, taking into account a short, an intermediate, and a large shoulder width. Measuring the range of the corona in terms of $\lambda\sigma$ (where σ is the hard core diameter) we have assumed the following specific values for the three cases: $\lambda=1.5$, $\lambda=4.5$, and $\lambda=10$. Investigating the system in the *NPT* ensemble we have searched for ordered particle configurations that minimize the Gibbs free energy; this means that the internal energy is minimized while the particle density is simultaneously maximized. These particle arrangements have been identified by means of a search strategy that is based on ideas of GAs. With this reliable, flexible, and efficient optimization tool at hand and taking benefit of the simple functional form of the interparticle potential, which considerably facilitates both numerical calculations as well as geometrical interpretations, we give evidence that the sequences of emerging particle configurations of minimum energy are complete.

A first look on the total of configurations gives clear indications that the formation of the particle arrangements follows well-defined rules as the pressure is increased: while at low pressure values the system prefers to form clusters, which populate the positions of low-symmetry lattices, we encounter at medium pressure values columnar and then lamellar structures. As a rule of the thumb we found that the distances between clusters, columns, and lamellas are always roughly equal to the shoulder width. Finally, at high pressure values, rather compact particle configurations are identified, which are in general characterized by a large number of near-

est neighbors. While this rule for the structural ordering might be still less obvious for small values of λ, it becomes more apparent with increasing range of the corona: at the intermediate λ value of 4.5, it is disobeyed only at two occasions, and for $\lambda=10$ the ordered particle configurations fully match this rule.

The large variety of ordered equilibrium configurations that have been identified is overwhelming. It represents an impressive example of the capacity and propensity of soft matter particles to self-organize in highly nontrivial structures. For demonstration we pick out two particular examples: first a cluster structure, where the clusters are composed of 22 particles, which, in turn, populate the positions of a triclinic lattice; second a columnar structure, where the particles align in a complex, helical column.

The particular shape of the repulsive shoulder, i.e., its flat energetic plateau in combination with the well-defined range of the corona, provides in addition the unique possibility to understand the system's strategy to form these complex structures. A detailed structural and energetical analysis of the emerging configurations reveals that the shoulder width plays the dominant role in this process; however, also the hard core can have considerable influence on the structure formation since it represents a lower boundary to interparticle distances. Thus, this study can be viewed as a pedagogical example which provides a deeper insight why particles arrange at a given state point in a particular structure, a knowledge that might be helpful in the investigations of self-assembly processes of systems with more complex interparticle potentials.

What are the next steps? The most obvious extension should be directed toward the investigations of the phase diagram at finite temperatures, i.e., one should address the question which of these configurations will "survive" at $T>0$. The theoretical route to this answer is quite straightforward: one has to "simply" merge the proposed search strategy with a suitable method to evaluate the thermodynamic properties of the system at a finite temperature. The obvious candidate to evaluate the thermodynamic properties of the system is of course classical density functional theory.[48] However, we have to raise immediately two serious concerns. First, no reliable density functional format for the square-shoulder system is available at present; treating, alternatively, the hard core within a suitable fundamental measure theory format (as, e.g., the one proposed in Ref. 49) and considering the shoulder by a mean-field-type perturbative approach risks providing data that are not sufficiently accurate to reliably distinguish between energetically competitive structures. Second, in search strategies based on ideas of GAs, the evaluation of the fitness function for an individual represents the numerical bottleneck in this approach. According to our experience, a combination of classical density functional theory with this particular search strategy might still be too time consuming for present-day computers. Alternatively to the theoretical route one might of course perform computer simulations and we point out that recently investigations in this direction have been performed on a related system.[50]

ACKNOWLEDGMENTS

The authors are indebted to Julia Fornleitner and Dieter Gottwald (both Wien) for stimulating discussions and for computational aid. Financial support by the Austrian Science Foundation under Project Nos. W004, P17823-N08, and P19890-N16 is gratefully acknowledged.

[1] P. C. Hemmer and G. Stell, Phys. Rev. Lett. **24**, 1284 (1970).
[2] J. M. Kincaid, G. Stell, and C. K. Hall, J. Chem. Phys. **65**, 2161 (1976).
[3] J. M. Kincaid, G. Stell, and E. Goldmark, J. Chem. Phys. **65**, 2172 (1976).
[4] C. Rascón, E. Velasco, L. Mederos, and G. Navascués, J. Chem. Phys. **106**, 6689 (1997).
[5] P. Bolhuis and D. Frenkel, J. Phys.: Condens. Matter **9**, 381 (1997).
[6] A. Lang, C. N. Likos, M. Watzlawek, and H. Löwen, J. Phys.: Condens. Matter **12**, 5087 (2000).
[7] E. Velasco, L. Mederos, G. Navascués, P. C. Hemmer, and G. Stell, Phys. Rev. Lett. **85**, 122 (2000).
[8] E. Jagla, Phys. Rev. E **58**, 1478 (1998).
[9] E. Jagla, J. Chem. Phys. **110**, 451 (1999).
[10] M. R. Sadr-Lahijany, A. Scala, S. V. Buldyrev, and H. E. Stanley, Phys. Rev. Lett. **81**, 4895 (1998).
[11] E. A. Jagla, J. Chem. Phys. **111**, 8980 (1999).
[12] Z. Yan, S. V. Buldyrev, N. Giovambattista, P. G. Debenedetti, and H. E. Stanley, Phys. Rev. E **73**, 051204 (2006).
[13] P. Kumar, S. V. Buldyrev, F. Sciortino, E. Zaccarelli, and H. E. Stanley, Phys. Rev. E **72**, 021501 (2005).
[14] Z. Yan, S. V. Buldyrev, N. Giovambattista, and H. E. Stanley, Phys. Rev. Lett. **95**, 130604 (2005).
[15] G. Malescio and G. Pellicane, Nat. Mater. **2**, 97 (2003).
[16] G. Malescio and G. Pellicane, Phys. Rev. E **70**, 021202 (2004).
[17] M. Glaser, G. Grason, R. Kamien, A. Košmrlj, C. Santangelo, and P. Ziherl, Europhys. Lett. **78**, 46004 (2007).
[18] J. Fornleitner and G. Kahl, Europhys. Lett. **82**, 18001 (2008).
[19] G. J. Pauschenwein and G. Kahl, Soft Matter **4**, 1396 (2008).
[20] P. Ziherl and R. Kamien, J. Phys. Chem. B **105**, 10147 (2001).
[21] Y. Norizoe and T. Kawakatsu, Europhys. Lett. **72**, 583 (2005).
[22] C. Pierleoni, C. Addison, J.-P. Hansen, and V. Krakoviack, Phys. Rev. Lett. **96**, 128302 (2006).
[23] A. Campbell, V. Anderson, J. van Duijneveldt, and P. Bartlett, Phys. Rev. Lett. **94**, 208301 (2005).
[24] P. Camp, Phys. Rev. E **68**, 061506 (2003).
[25] A. de Candia, E. D. Gado, A. Fierro, N. Sator, M. Tarzia, and A. Coniglio, Phys. Rev. E **74**, 010403(R) (2006).
[26] A. Stradner, H. Sedgwick, F. Cardinaux, W. C. K. Poon, S. U. Egelhaaf, and P. Schurtenberger, Nature (London) **432**, 492 (2004).
[27] B. Mladek, D. Gottwald, G. Kahl, M. Neumann, and C. Likos, Phys. Rev. Lett. **96**, 045701 (2006).
[28] B. Mladek, D. Gottwald, G. Kahl, M. Neumann, and C. Likos, Phys. Rev. Lett. **97**, 019901(E)(2006).
[29] J. Holland, *Adaption in Natural and Artificial Systems* (The University of Michigan, Ann Arbor, 1975).
[30] S. M. Woodley, P. D. Battle, J. D. Gale, and C. R. A. Catlow, Phys. Chem. Chem. Phys. **1**, 2535 (1999).
[31] A. R. Oganov and C. W. Glass, J. Chem. Phys. **124**, 244704 (2006).
[32] A. R. Oganov and C. W. Glass, J. Phys.: Condens. Matter **20**, 064210 (2008).
[33] D. Gottwald, C. Likos, G. Kahl, and H. Löwen, Phys. Rev. Lett. **92**, 068301 (2004).
[34] D. Gottwald, G. Kahl, and C. Likos, J. Chem. Phys. **122**, 204503 (2005).
[35] D. Gottwald, C. Likos, G. Kahl, and H. Löwen, J. Chem. Phys. **122**, 074903 (2005).
[36] J. Fornleitner, F. Lo Verso, G. Kahl, and C. N. Likos, Soft Matter **4**, 480 (2008).
[37] G. J. Pauschenwein and G. Kahl (unpublished).
[38] M. J. D. Powell, Comput. J. **7**, 155 (1964).
[39] Note that the formation of nontrivial close-packed arrangements is also reported for certain rare earth elements (page 79 in Ref. 40).
[40] N. W. Ashcroft and N. D. Mermin, *Solid State Physics* (Saunders, Philadelphia/Harcourt, Brace, New York, 1976).
[41] G. J. Pauschenwein, Ph.D. thesis, Institut für Theoretische Physik, TU Wien, 2008.

[42] This choice is motivated by the fact that—although the stacking sequence for fcc is longer than the one for hcp—the crystallographic description for the fcc requires only one basis particle, while for the hcp structure it is a nonsimple one.
[43] C. N. Likos, M. Watzlawek, and H. Löwen, Phys. Rev. E **58**, 3135 (1998).
[44] C. N. Likos, A. Lang, M. Watzlawek, and H. Löwen, Phys. Rev. E **63**, 031206 (2001).
[45] B. M. Mladek, G. Falkinger, and G. Kahl (unpublished).
[46] C. N. Likos, B. M. Mladek, D. Gottwald, and G. Kahl, J. Chem. Phys. **126**, 224502 (2007).
[47] B. M. Mladek, D. Gottwald, G. Kahl, M. Neumann, and C. N. Likos, J. Phys. Chem. B **111**, 12799 (2007).
[48] R. Evans, *Fundamentals of Inhomogeneous Fluids* (Marcel Dekker, New York, 1992), Chap. 3, pp. 85–175.
[49] R. Roth, R. Evans, A. Lang, and G. Kahl, J. Phys.: Condens. Matter **14**, 12063 (2002).
[50] Y. D. Fomin, N. V. Gribova, V. N. Ryzhov, D. Frenkel, and S. M. Stishov, J. Chem. Phys. **129**, 064512 (2008).